Article ID: 1006-8775(2015) 01-0084-08

MODELING AND QUANTITATIVE RETRIEVAL OF FINITE FIELD FOR THE TROPICAL SEA SURFACE WIND SPEED OF THE FY–3B MICROWAVE IMAGER

AN Da-wei (安大伟), LU Feng (陆 风), DOU Fang-li (窦芳丽), ZHANG Peng (张 鹏)
(National Satellite Meteorological Center, China Meteorological Administration, Beijing 100081 China)

Abstract: The purpose of this study is to select a suitable sea wind retrieval method for FY-3B (MWRI). Based on the traditional empirical model of retrieving sea surface wind speed, and in the case of small sample size of FY-3B satellite load regression analysis, this paper analyzes the channel differences between the FY-3B satellite microwave radiation imager (MWRI) and TMI onboard the TRMM. The paper also analyzes the influence of these differences on the channel in terms of receiving temperature, including channel frequency, sensitivity and scaling precision. Then, the limited range of new model coefficient regression analysis is determined (in which the channel range settings include the information and features of channel differences), the regression methods of the finite field are proposed, and the empirical model of wind speed retrieval applicable to MWRI is obtained, which achieves robust results. Compared to the TAO buoy data, the mean deviation of the new model is 0.4 m/s, and the standard deviation is 1.2 m/s. In addition, the schematic diagram of the tropical sea surface wind speed retrieval is provided.

Key words: microwave radiometry; tropical sea surface wind; MWRI; FY-3B
CLC number: P414.4 **Document code:** A

1 INTRODUCTION

The successful launch of the FY-3B satellite in 2010 has provided a favorable platform for the improvement of satellite microwave radiometers in terms of measuring the speed of sea surface wind field and aided in subsequent data collection. The radiation energy of the microwave band at ocean surface depends highly upon the geometry parameters of the sea surface, such as wave structure and foam coverage (Ulaby [1] et al.). Accordingly, a significant causal relationship exists between the sea surface wind field and the formation and evolution of the parameters. Over the past thirty years, researchers in the field of microwave remote sensing technology have made great efforts to more efficiently identify sea surface wind and the microwave energy of satellite-borne surface radiation. In addition to this, a buoy (Xu et al.[2]) currently travelling across the global coverage also provides accurate verification standards for application to satellite-borne instruments.

Many researchers from around the world have measured sea surface wind fields using satellite technology. For example, applications of active radar instruments and ordinary scattermeters (such as QuikSCAT/Seawinds and METOP/ASCAT) have achieved considerable success, and passive radiometers have been used to measure these wind fields (Alsweiss et al.[3]; Singh et al.[4]; Wang[5]; Li[6]; Liu and He[7]). Moreover, in order to obtain the sea surface wind field speed, a D-matrix algorithm was developed and correlation studies were carried out using the brightness temperature channels of a microwave imager (SSM/I) as well as other instruments (Goodberlet et al.[8]; Goodberlet and Swift[9]; Chang and Li[10]; Hwang[11]; Bobylev et al.[12]). However, although the wind speed (WS) retrieval accuracy provided by the new D-matrix algorithm has been greatly improved, it is still quite sensitive to atmospheric interference and effective only under the condition of being "without rain". Most of the interference occurs in the transmission paths which have high microwave frequencies. For example, the frequency channels used by SSM/I are concentrated in the frequencies of 37.0, 22.235, 19.35 and 85.5 GHz. In fact, when taking the sensitivity to cloud and rain into consideration, the radiometer has a low frequency (10 GHz) polarization channel which is capable of penetrating various atmospheric conditions. The WindSat radiometer uses the polarimetric radiometer channel of 10.7 GHz to assist in measuring sea surface wind after penetrating complex atmospheric conditions. Many studies similar to this one have been conducted in China as well (Wang and Li[13]; Lin and Mao[14]; Li et al.[15]; An et al.[16]).

Laurence and Chang [17] used the TMI radiometer with a 10.7 GHz channel on the TRMM satellite and achieved robust results. However, due to the settings of mid- and low-latitude orbit of the TRMM satellite, it is

Received 2013-09-09; **Revised** 2014-10-29; **Accepted** 2015-01-15
Foundation item: Foundation item: National Science Foundation of China (41105009, 41175023); Ministry of Science and Technology, China (2010DFA21140)
Biography: AN Da-wei, Ph.D., associate professor, primarily undertaking research on sea surface wind and microwave calibration.
Corresponding author: AN Da-wei, e-mail: andawei@cma.gov.cn

difficult to accurately extract the global sea surface WS using this satellite, thus limiting its application.

In the present study, the microwave radiation imager MWRI on the FY-3B satellite of the China Meteorological Administration was used. The frequencies of the instrumental channels were 10.65, 18.7, 23.8, 36.5 and 89 GHz, with rich channel settings. The imager was not only equipped with high-frequency channels similar to those of SSM/I, but also with the 10.7 GHz channel, which is able to penetrate atmospheric conditions. In addition, due to the fact that the FY-3B was a polar orbit satellite, the instrument had the capability of extracting global sea surface WS. In this study, based on the traditional empirical model of retrieving sea surface WS, the channel differences between the FY-3B satellite microwave radiation imager (MWRI) and TMI are analyzed, as is the influence of the differences on the channel. The results provided the temperature, with the sample of the FY-3B satellite load regression analysis significantly small in size. Then the limited range of new model coefficient regression analysis is set (the settings of the channel range include the information and features of channel differences), and the regression methods of the finite field are proposed, using 2011 MWRI data and Tropical Atmosphere Ocean (TAO) buoy data (See Fig. 1) obtained with the empirical model of WS retrieval applicable to MWRI, the results of which are quite robust. The schematic diagram of tropical sea surface WS retrieval is created, using 2012 MWRI data and TAO buoy data to verify the accuracy and usefulness of the model, thus providing new methods for China to measure tropical sea surface WS using FY-3B satellite load microwave radiometers.

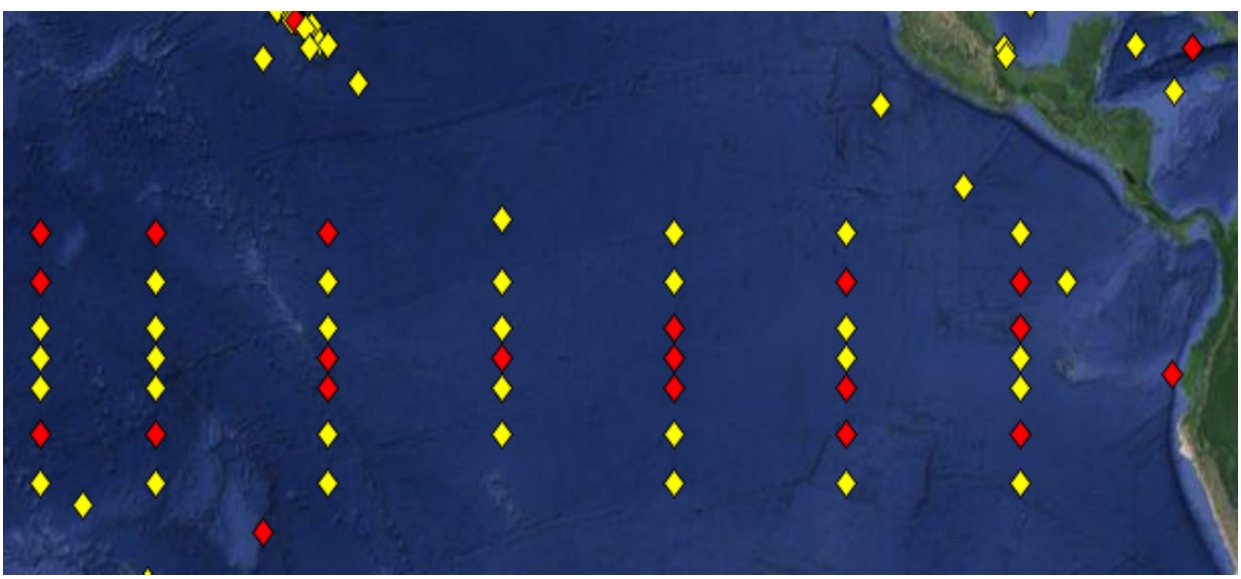

Figure 1. Distribution of Tropical Atmosphere Ocean (TAO) buoys.

2 DATA SOURCE AND MATCHING

MWRI is a dual-polarization microwave radiometer containing five frequencies, namely 10.65, 18.7, 23.8, 36.5 and 89 GHz. There are similar settings on SSM/I, but the newly increased GHz channel and the 23.8 GHz water vapor channel of the MWRI may assist in resolving the problem of the MWRI when measuring cloudy and rainy areas. The antenna beam of the MWRI is equipped with conical scanning and the resolution views (EFOV) of all channels range from 10 to 80 km. The circular orbit altitude is 836 km, the antenna perspective is 45 degrees, and the ground width is 1 400 km, thus it has excellent capability of covering the entire globe.

In this study, the sea surface wind data were measured by the offshore TAO buoy from the National Data Buoy Center of NOAA (National Oceanic and Atmospheric Administration, USA). Development of the Tropical Atmosphere Ocean (TAO) array was motivated by the 1982-1983 El Nino event, which highlighted the need for real-time data from the tropical Pacific. All WS measurements were adjusted to 19.5 m above sea level, and the height level was important for the comparison between buoys and the estimation of the traditional D-matrix. Based on the D-matrix developed by Connor and Chang[17], one matching constraint was the MWRI brightness temperature: the position difference of the buoy WS was less than 15 km and the time difference was less than 15 min. Another constraint was that only one data group was allowed for each flight in order to ensure the independence of the samples. Therefore, the buoys closest to the pixel of the MWRI ground track were selected. In order to avoid land pollution on brightness temperature, the buoy data was effective when the distance between the land and buoy was greater than 100 km. These standards resulted in the matching of 50 available TAO buoys and 3 193 instances in 2011 and 924 instances in 2012.

3 MODELING RESEARCH

3.1 *Analysis of model and results*

The fundamental assumption of the D-matrix algorithm is the geophysical parameters it requires. For example, sea surface WS may be expressed as the linear combination of brightness temperature, which is the general form shown in Eq. (1).

$$WS=C_0+C_1T_{B1}+C_2T_{B2}+\cdots+C_NT_{BN} \quad (1)$$

where C is the coefficient and T the brightness temperature. The subscripted TB variables shown in Eq. (1) are the brightness temperatures associated with the channels chosen for the algorithm, and the subscripted C is the coefficient determined via regression analysis. The algorithmic variables shown in Eq. (1)are related to the brightness temperature and selected channel, and the coefficients are determined by means of regression analysis. The global WS algorithm proposed by Connor and Chang[17] used the 10 V(vertical polarization), 19 V (horizontal polarization), 21 V, 37 V and 37 H channels of the TRMM, and the forms are as follows:

$$\begin{aligned}\mathrm{WS}=&C_0+C_1T_B(10\mathrm{V})+C_2T_B(10\mathrm{H})+C_3T_B(19\mathrm{V})\\&+C_4T_B(21\mathrm{V})+C_5T_B(37\mathrm{V})+C_6T_B(37\mathrm{H})\end{aligned} \quad (2)$$

However, this algorithm does not apply to the retrieval of sea surface WS using the MWRI of FY-3B. The algorithm requires correction so as to establish a new model by which the WS retrieval of the MWRI is carried out. For the two satellites equipped with the same radiometer channel, the channel brightness temperature of the radiation contribution is not absent, but the center frequency has some minor differences, which can be equivalent to frequency drift that affects the accuracy of the product, in which case the TMI equation topology can be directly applied but must be optimized for each channel coefficient.

$$\begin{aligned}\mathrm{WS}=&C_0+C_1T_B(10.65\mathrm{V})+C_2T_B(10.65\mathrm{H})+C_3T_B(18.7\mathrm{V})\\&+C_4T_B(21.8\mathrm{V})+C_5T_B(36.5\mathrm{V})+C_6T_B(36.5\mathrm{H})\end{aligned} \quad (3)$$

In order to determine the coefficients, multiple linear regression analysis was used for respectively measuring the WS and matching the buoy WS to the five brightness temperature channels of the MWRI. When determining the coefficients, the valid data rain sign is 0 and the invalid data rain sign is 1, by using the comparison of the MWRI. The precipitation detection threshold based on the TMI was adjusted (with the range expanded) to ensure that the MWRI-retrieved RMS was superior to that of TMI (RMS: 1.46 m/s), the adjusted valid data (rain=0) increased by 30%, and the invalid data is reduced, but the overall accuracy of the product is reduced (1.2 m/s to 1.41 m/s), therefore it is necessary to strike a balance between accuracy and threshold range. This paper considers accuracy a priority and thus uses a threshold of TMI. The conditions for proposing rain signs are shown in Table 1.

As is widely known, the sea surface WS distributed throughout the world is uneven and asymmetrical, and 95% of the WS is mainly concentrated within the range of 2 to 15 m/s. The algorithm model structure of wind field retrieval shown in Eq. (3) was used.

Table 1. Rain signs distribution.

rain sign	Condition
0	$T_B(36.5V)-T_B(36.5H)>42K$ and $T_B(18.7H)<200K$
1	$37K<T_B(36.5V)-T_B(36.5H)<42K$ or $T_B(18.7H)>200K$

3.2 *Regression analysis of finite field based on the differences in the instrument indicators*

Regression analysis is the statistical analysis method used to study the dependence relations between a random variable (Y) and another variable (X) or a group of variables (X_1, X_2, $\cdots$, X_k). The analysis of a large amount of data is required, often tens of thousands of data points. However, the time period for the MWRI of FY-3B to be in the orbit is quite short, and not enough diverse data is available for comprehensive fitting. Therefore, the regression method of a finite field was considered, i.e. a model based on the preliminary model of TMI with channel settings similar to those of the MWRI was established (the preliminary model of TMI has universality after a large amount of data fitting). Then fine adjustment was conducted for the coefficients according to channel frequency, sensitivity and other factors. Finally, the new retrieval model applicable to the MWRI was established.

The regression analysis model is as follows:

$$\begin{cases}\mathrm{WS}=TC+C_0\\ \mathrm{E}(C_0)=0,\mathrm{COV}(C_0,C_0)=\sigma^2I_n\end{cases} \quad (4)$$

$$\mathrm{WS}=\begin{bmatrix}ws_1\\ \cdots\\ \cdots\\ ws_n\end{bmatrix},\ T=\begin{bmatrix}1t_{11}t_{12}\ldots t_{1k}\\ 1t_{21}t_{22}\ldots t_{2k}\\ \ldots\ldots\ldots\ldots\\ 1t_{n1}t_{n2}\ldots t_{nk}\end{bmatrix},\ C=\begin{bmatrix}c_0\\ c_1\\ \cdots\\ c_k\end{bmatrix},$$

$$C_0=\begin{bmatrix}c_{01}\\ c_{02}\\ \cdots\\ c_{0n}\end{bmatrix},\ \text{where}\ \ \mathrm{WS}=C_0+C_1t_1+\ldots+C_kt_k$$

is a regression plane equation. T is the brightness temperatures, the C_s are the coefficients, E(x) is the expected value, and COV (x,y) are the covariances. The linear model (WS,TC,σ^2I_n) was mainly used to analyze the point estimation and hypotheses testing of unknown parameters C and σ^2 using test values, thus establishing

the quantitative relations between WS and $t_1t_2\cdots t_k$. Then the value of WS at the place of $t_1=t_{01}, t_2=t_{02}, \cdots, t_k=t_{0k}$ was predicted and controlled, i.e. interval estimation for WS was conducted. Based on the concept of least squares, the sum of squares was shown to be $Q=\sum_{i=1}^{n}(ws_i-c\times t_i-c_0)$. Consequently, the linear regression equation coefficients of c and c_0, when the value of Q was smallest, were provided. Meanwhile, the values of c and c_0 are within a certain range of the initial value of the original model:

$$\begin{cases} c=\dfrac{\sum_{i=1}^{n}(t_i-\bar{t})(ws_i-\bar{ws})}{\sum_{i=1}^{n}(t_i-\bar{t})^2}=\dfrac{\sum_{i=1}^{n}t_i\times ws_i-n\bar{t}\times\bar{ws}}{\sum_{i=1}^{n}t_i^2-n\bar{t}^{-2}} \\ c_0=\bar{ws}-c\times\bar{t};....;e_i<c_i<ee_i;i\in[0,k] \end{cases} \quad (5)$$

where c_i is the coefficient, c_0 is the constant coefficient, and $t_1t_2\cdots t_k$ are the brightness temperatures. The key is the selection of coefficient c_i within the fluctuating range. c_i fluctuates within the set range by taking the initial value of the corresponding coefficient for adjustment to make the value of Q reach the minimum value (non-traditional regression method causes the value of Q to become 0), and the fluctuating range is obtained by means of weighing.

It may be seen that differences exist between the two instruments of Table 2 in terms of the corresponding channel frequency, sensitivity and calibration accuracy. This is due to the fact that the differences between the channels will influence the temperature data collected by the various instruments. Based on these differences, weighted design was conducted. Finite field regression was conducted for the coefficients. For the channels with small differences, the changes in the corresponding coefficients were small; for those with large differences, the changes in the corresponding coefficients were large.

Table 2. MWRI, TMI channel parameters.

Instrument	T		M		T	M	T	M	T		M	
Frequency /GHz	10.7		10.65		19.4	18.7	21.3	23.8	37		36.5	
	V	H	V	H	V	V	V	V	V	H	V	H
Sensitivity /K	0.63	0.54	0.5	0.54	0.5	0.5	0.71	0.8	0.36	0.5	0.31	0.5
Accuracy of calibration /K	1	1	1	1	1.5	2	1.5	2	1.5	1.5	2	2
Influence coefficient	c_1	c_2	c_1	c_2	c_3	c_3	c_4	c_4	c_5	c_6	c_5	c_6

The respective differences in channel frequency f, sensitivity ΔK and calibration accuracy K were then analyzed.

For monochromatic frequency f, transmittance is the exponential function of the optical thickness.

$$\underset{v}{T}(p_s,p)=\exp[-\frac{1}{g}\int_{p}^{p_s}\underset{v}{k}(p')q(p')dp'] \quad (6)$$

where T is the optical thickness, k is the extinction coefficient, q is the density mixing ratio, and g is the gravitational acceleration. It may be seen from the two-dimensional function curve relationship between the transmission ratio and frequency that the transmission ratio shows the characteristic of monotonically decreasing the function near the frequencies of 10, 19 and 37 GHz. At the points located close to the frequency point, the lower the frequency is, the smaller the attenuation will be; in addition, the smaller the attenuation is, the greater the coefficient weighing caused by frequency at the frequency point will be.

For sensitivity ΔK, the more sensitive the channel is, the greater the coefficient weighing caused by sensitivity at the frequency point will be.

For calibration accuracy K, the higher the accuracy is, the greater the coefficient weighing caused by accuracy at the frequency point will be.

The specific coefficients are distributed based on the weighing of channel frequency f, sensitivity ΔK and calibration accuracy K.

The following Eqs are the threshold adjustment of the original coefficient based on channel frequency f, sensitivity ΔK and calibration accuracy K. Eq. (7) is used to describe a range of limited iteration intervals, and if the frequency, sensitivity and calibration accuracy are the same, then the contribution of this weighting is 0; if the difference is greater, then the weighted contribution and influence coefficient iteration range will be larger as well. The adjustment process of the new coef ficient is as follows.

$$C_0' = C_0$$

$$C_1' = C_1 \times (1 + \frac{f_{T10V} - f_{M10V}}{f_{T10V}} + \frac{\Delta K_{T10V} - \Delta K_{M10V}}{\Delta K_{T10V}} + \frac{K_{T10V} - K_{M10V}}{K_{T10V}})$$

$$C_2' = C_2 \times (1 + \frac{f_{T10H} - f_{M10H}}{f_{T10H}} + \frac{\Delta K_{T10H} - \Delta K_{M10H}}{\Delta K_{T10H}} + \frac{K_{T10H} - K_{M10H}}{K_{T10H}})$$

$$C_3' = C_3 \times (1 + \frac{f_{T19V} - f_{M19V}}{f_{T19V}} + \frac{\Delta K_{T19V} - \Delta K_{M19V}}{\Delta K_{T19V}} + \frac{K_{T19V} - K_{M19V}}{K_{T19V}}) \quad (7)$$

$$C_4' = C_4 \times (1 + \frac{f_{T21V} - f_{M21V}}{f_{T21V}} + \frac{\Delta K_{T21V} - \Delta K_{M21V}}{\Delta K_{T21V}} + \frac{K_{T21V} - K_{M21V}}{K_{T21V}})$$

$$C_5' = C_5 \times (1 + \frac{f_{T37V} - f_{M37V}}{f_{T37V}} + \frac{\Delta K_{T37V} - \Delta K_{M37V}}{\Delta K_{T37V}} + \frac{K_{T37V} - K_{M37V}}{K_{T37V}})$$

$$C_6' = C_6 \times (1 + \frac{f_{T37H} - f_{M37H}}{f_{T37H}} + \frac{\Delta K_{T37H} - \Delta K_{M37H}}{\Delta K_{T37H}} + \frac{K_{T37H} - K_{M37H}}{K_{T37H}})$$

where C' is the intermediate value of the coefficient, and C is the original coefficient. Based on the threshold adjustment shown in Eq. (8), the limited regression range of each corresponding new coefficient is obtained. The finite field range settings of the coefficients include the information and features of the channel differences. Therefore, the new coefficient range is as follows:

$$C_0'' \in [C_0 - |C_0 - C_0'|, ..., C_0 + |C_0 - C_0'|]$$

$$C_1'' \in [C_1 - |C_1 - C_1'|, ..., C_1 + |C_1 - C_1'|]$$

$$C_2'' \in [C_2 - |C_2 - C_2'|, ..., C_2 + |C_2 - C_2'|]$$

$$C_3'' \in [C_3 - |C_3 - C_3'|, ..., C_3 + |C_3 - C_3'|] \quad (8)$$

$$C_4'' \in [C_4 - |C_4 - C_4'|, ..., C_4 + |C_4 - C_4'|]$$

$$C_5'' \in [C_5 - |C_5 - C_5'|, ..., C_5 + |C_5 - C_5'|]$$

$$C_6'' \in [C_6 - |C_6 - C_6'|, ..., C_6 + |C_6 - C_6'|]$$

where C_s'' are the final coefficients for each calculation loop. The specific algorithm process is as follows. Fig. 2 is described as follows: First, combine the initial TMI coefficient with Eq. (7) and give a limited scope of the channel coefficients iteration, then generate the retrieved WS data sets, and the corresponding sea buoy wind data sets are compared; fix a new combination of coefficients C", and a further iteration adjustment cycle will proceed until preset accuracy can be achieved.

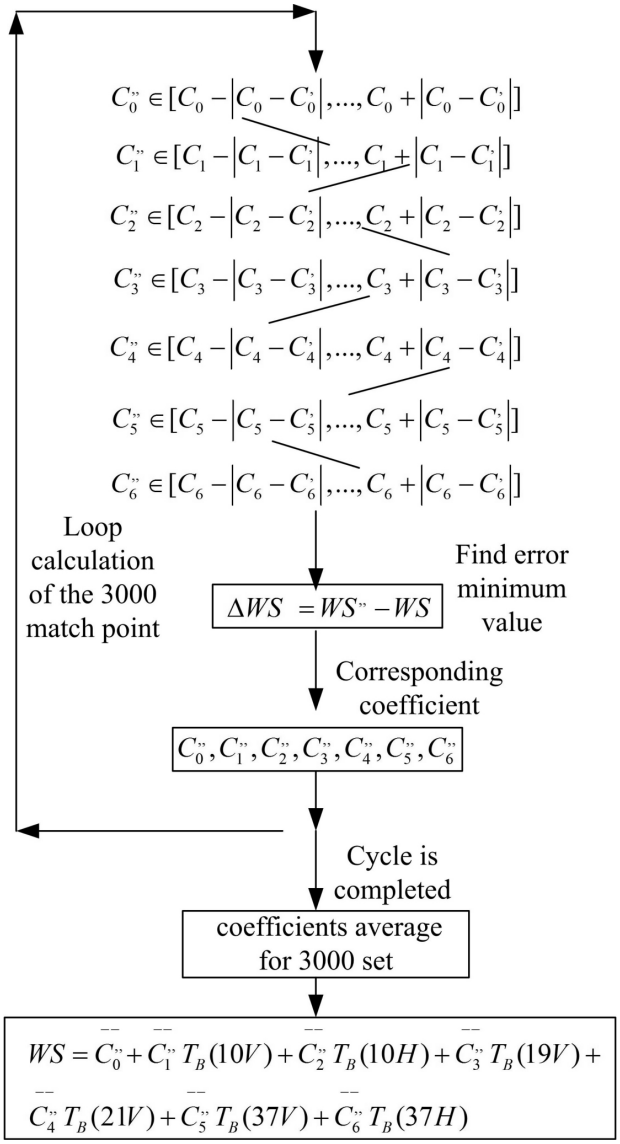

Figure 2. Finite field regression.

Therefore, the new model structure is as follows:

$$\mathrm{WS} = \bar{C_0''} + \bar{C_1''} T_B(10\mathrm{V}) + \bar{C_2''} T_B(10\mathrm{H}) + \bar{C_3''} T_B(19\mathrm{V}) + \bar{C_4''} T_B(21\mathrm{V}) + \bar{C_5''} T_B(37\mathrm{V}) + \bar{C_6''} T_B(37\mathrm{H}) \quad (9)$$

where WS is the WS for the new model, and the C_s'' are the average of all loops and the final coefficients. The new finite field regression coefficient is shown in Table 3.

A series of finite field regression were conducted according to the specified process, the design of the D-matrix algorithm structure, as shown in Eq. (3), was optimized, and a new WS model, as shown in Eq. (10), was obtained.

3.3 *Verification*

The error scatterplot is shown in Fig. 3. Brightness temperature data were obtained from WMRI to determine the algorithm model of wind field retrieval. Then,

924 fitting data of the MWRI buoy for 2012 were collected, the rain signs of which were all 0, and the MWRI WS (shown in Fig. 3) and the buoy WS scatterplot of corresponding time and space were generated (in which the x-coordinates represent the buoy WS). After the optimization, the error between the true value and the WS inverted by MWRI was identified. The mean value was 0.4 m/s, the variance was 1.1 $(m/s)^2$ and the root mean square (RMS) was 1.2 m/s (TMI on the TRMM: RMS was 1.46 m/s), and the correlation coefficient was 0.88. Brightness temperature channel error had greater impact on retrieval error and 37V and 37H had the greatest impact on the retrieval errors. Two channels distributed around the area of the window channels, and the shorter the wavelength, more sensitive the roughness of the sea surface reflection is, followed by 10V and 10H, but 19V and 21V almost had no effect. Design results met the design requirements accuracy (3 m/s) and even reached the precision for radar scatterometer wind products.

The following is the global sea surface WS for September 28, 2011 based on the new model structure, which is inverted by the MWRI data carried by FY3B. The second diagram shows the AMSR-E surface WS, where the white circle represents a typical and similar WS region. There are some differences in color code and track scanning positions. The white circle represents a typical and similar WS region (with low WS over the Atlantic surface, high WS over the Southwest Pacific surface, and with low WS over the Indian Ocean surface).

Table 3. Distribution of new model coefficients.

Band	Coefficient	Value
content	$C_0^{''}$	101.5096
10V	$C_1^{''}$	0.2887
10H	$C_2^{''}$	0.1209
19V	$C_3^{''}$	0.0332
21V	$C_4^{''}$	0.0229
37V	$C_5^{''}$	-1.1578
37H	$C_6^{''}$	0.5128

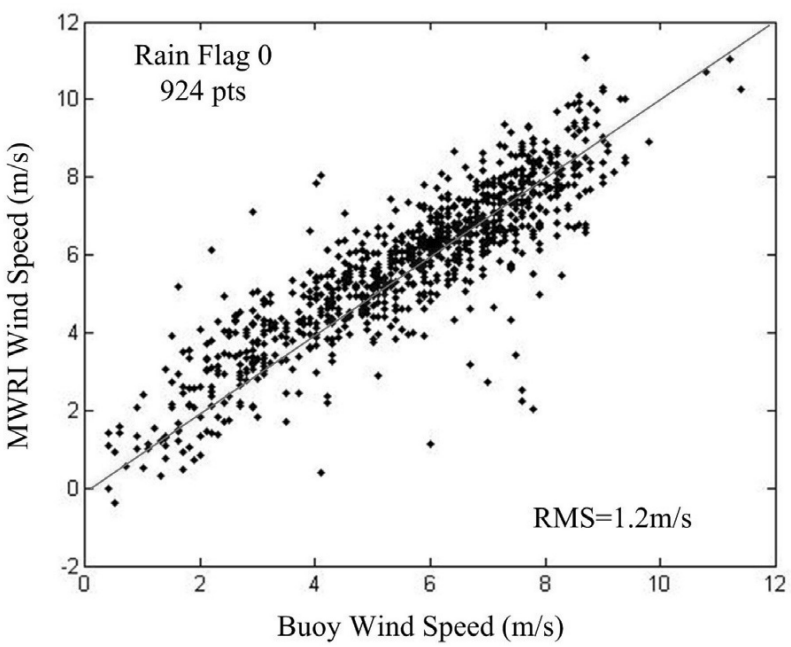

Figure 3. Scatter plot of buoy WS versus retrieved WS from MWRI observations using the new mode (with the correlation coefficient at 0.88).

As shown in Fig. 4, the WS range is 0 to 14 m/s and the blank area within the scanning range is the rain area, with a rain sign of 1; for the data in other areas, the rain sign is 0. The red area represents strong wind while the blue area represents weak wind. It may be seen that the strong wind area is mainly concentrated in high-latitude sea regions while the weak wind area is mainly concentrated in low-latitude marine regions. In addition, the distribution of WS alters with the latitude.

4 CONCLUSIONS

This paper first introduces the development progress and recent re sults of an empirical model of satellite-loaded microwave meter to invert sea surface WS, then presents the matching of data sources, including the introduction to the MWRI instrument and verification of the buoy data. The brightness temperature data of the FY-3B satellite microwave imager (MWRI)

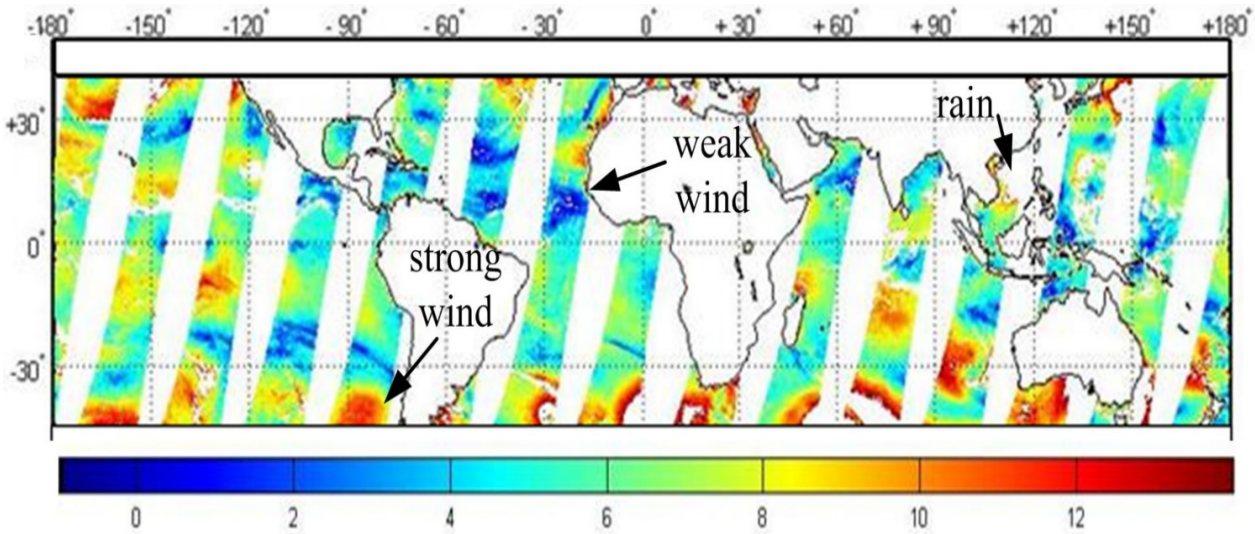

Figure 4. Global tropical sea surface WS retrieval results from MWRI measurements on September 28, 2011. MWRI rain flag definitions and the new model algorithm were used for WS retrieval. Only rain flag zero data is shown.

throughout a whole year are analyzed, and the WS retrieval results of the original TMI model applied to the MWRI are provided. Subsequently, the channel differences between the FY-3B satellite microwave imager (MWRI) and TMI are analyzed, as are the influences of the differences on the channel to receive temperature, including channel frequency f, sensitivity $\triangle K$ and scaling precision K. The limited range for setting the new model coefficient regression analysis is analyzed and set (the settings of channel range include the information and features of channel differences), the regression method of the finite field is proposed, the algorithm process of the finite field is provided, and the new WS retrieval model applicable to the FY-3B MWRI of China for tropical sea wind is obtained, from which robust results are achieved. Here is how the method given in this paper works: When the channel is the same, only fine adjustments are made in the new instrument retrieval method without the need to search for a new re trieval equation. This paper shows that when the accuracy is greater than 3 m/s, winds can be directly applied to the FY-3B service system and atmospheric dynamical parameters on the sea surface and protection of related human activities has practical significance. According to the results of this paper, the optimal design of the pro posed new instrument is set to the 6.9 GHz channel, because atmospheric transmittance is better if done through a low-frequency channel, thus the future work will set the 6.9 GHz retrieval channel, which makes it possible to retrieve the rain area of sea wind.

Acknowledgement: The ASCAT sea surface wind data are provided by the User Service Helpdesk EUMETSAT User Service. Thanks to Pamela Schöbel-Pattiselanno, Anton Verhoef and the rest of the crew. The buoy data are provided by NOAA National Weather Service National Data Buoy Center.

REFERENCES:

[1] ULABY F T, MOORE R K, FUNG A K. Microwave remote sensing: active and passive [M]. Norwood: Artech House, 1986.

[2] XU Xiang-chun, XIN Ji-wu, LIANG Guo-feng, et al. Observation and analysis of sea surface wind over the Qiongzhou Strait [J]. J Trop Meteorol, 2010, 16 (4): 402-408.

[3] ALSWEISS S O, LAUPATTARAKASEM P, JONES W L. A novel Ku-band radiometer/scatterometer approach for improved oceanic wind vector measure ments [J]. IEEE Trans Geos Rem Sens, 2011, 49 (9): 3 189-3 197.

[4] SINGH R, KUMAR P, PAL P K. Assimilation of Oceansat-2-scatterometer-derived surface winds in the weather research and forecasting model [J]. IEEE Trans Geos Rem Sens, 2012, 50(4): 1 015-1 021.

[5] WANG Liang, LU Han-cheng, PAN Xiao-bin, et al. Correction of asymmetric strengthening of QuikSCAT wind field and assimilation application in typhoon simulation [J]. J Trop Meteorol, 2009, 15(1): 78-82.

[6] LI Jiang-nan, WANG An-yu, YANG Zhao-li, et al. DCT analysis distribution features of near-surface wind fields during the landfall of Vongfong [J]. J Trop Meteorol, 2003, 9(2): 143-151.

[7] LIU Chun-xia, HE Xi-cheng. The analysis on the statistical character of QuikSCAT scatterometer winds and strong wind frequency using remote sensor data from QuikSCAT [J]. J Trop Meteorol, 2003, 9(2): 113-123

[8] GOODBERLET M A, SWIFT C T, WILKERSON J C. Ocean Surface Wind Speed Measurements of the Special Sensor Microwave/Imager (SSM/I) [J]. IEEE Trans Geos Rem Sens. 1990, 28(5): 823-828.

[9] GOODBERLET M A, SWIFT C T. Improved Retrievals from the DMSP Wind Speed Algorithm Un der Adverse Weather Conditions [J]. IEEE Trans Geos Rem Sens, 1992, 30(5): 1 076-1 077.

[10] CHANG P S, LI Li. Ocean Surface Wind Speed and Direction Retrievals from the SSM/I [J]. IEEE Trans Geos

Rem Sens, 1998, 36(6): 1 866-1 871.
[11] HWANG P A. Foam and roughness effects on passive microwave remote sensing of the ocean [J]. IEEE Trans Geos Rem Sens, 2012, 50(8) 2 978-2 985.
[12] BOBYLEV L P, ZABOLOTSKIKH E V, MITNIK L M, et al. Arctic polar low detection and monitoring using atmospheric water vapor retrievals from satellite passive microwave data [J]. IEEE Trans Geos Rem Sens, 2011, 49(9): 3 302-3 310.
[13] WANG Zhen zhan, LI Yun. Geophysical parameters retrieving algorithm of AMSR [J]. J Rem Sens, 2009, 29 (4): 355-370.
[14] LIN Lei, MAO Zhi-hua. The wind speed retrieval by the microwave radiometer (SSMI) five channels data [J]. Chin J Sci Instr, 2008, 29(4): 170-172.
[15] LI LE-le, GUAN Lei, CHEN Rui. Study on an algorithm for the retrieval of oceanic and atmospheric parameters from satellite microwave radiometer measurements [J]. J Ocean Univ China, 2006, 36(Suppl.): 205-211.
[16] AN Da-wei, GU Song-yan, YANG Zhong-dong, et al. Ocean surface non-cyclone wind block ambiguity removal algorithm for scatterometer [J]. J Appl Meteorol Sci, 2012, 23 (4): 485-492. doi:10.3969/j.issn. 1001-7313.2012.04.012
[17] LAURENCE N C, CHANG P S. Ocean surface wind retrievals using the TRMM microwave imager [J]. IEEE Trans Geos Rem Sens, 2000, 38(4): 2 009-2 016.

Citation: AN Da-wei, LU Feng, DOU Fang-li, et al. Modeling and quantitative retrieval of finite field for the tropical sea surface wind speed of the FY-3B microwave imager [J]. J Trop Meteorol, 2015, 21(1): 84-91.